ACTIVATED MICROCRYSTALLINE CELLULOSE MATRICES BY EMBEDDING Ag AND TiO_2 NANOPARTICLES

LEONARD IGNAT, FLORICA DOROFTEI, ANDREI DASCĂLU and MAURUȘA-ELENA IGNAT

"Petru Poni" Institute of Macromolecular Chemistry,
Grigore Ghica-Voda Alley, No. 41A, Iasi, 700487, Romania
✉ *Corresponding author: M.-E. Ignat, mignat@icmpp.ro*

Received June 23, 2026

This study aimed to develop and evaluate microcrystalline cellulose (MCC)-based hybrid materials containing sodium lignosulfonate (LS), rutile TiO_2, and silver nanoparticles (AgNPs) for the removal of Basic Blue 41 (BB41) from aqueous solutions. The materials were characterized by FTIR, XRD, SEM and polarized optical microscopy, as well as in terms of elemental composition and spatial distribution of the constitutive elements. The obtained results indicated that the main structural features of cellulose were preserved after materials preparation, while the rutile crystalline phase was retained in TiO_2-containing materials. All products exhibited improved dye retention compared with unmodified MCC. After 300 min, MCC_LS_TiO_2_AgNPs achieved the highest adsorption capacity (64.88 mg/g) and removal efficiency (81.26%), compared with 43.93 mg/g and 55.29%, respectively, for pristine MCC. EDX results, together with the corresponding elemental distribution maps, support the successful preparation of the hybrid composites. These findings highlight the potential of the developed compounds as adsorbents for cationic dye removal from water.

Keywords: microcrystalline cellulose, sodium lignosulfonate, titanium dioxide, silver nanoparticles, hybrid materials, Basic Blue 41, cationic dye adsorption, wastewater treatment

INTRODUCTION

The contamination of aquatic environments with synthetic dyes represents a major environmental concern because of their extensive use in textile, paper, leather, and other industrial processes. Dye-containing wastewater can reduce light penetration, interfere with aquatic photosynthesis, and introduce potentially toxic, mutagenic, or carcinogenic compounds into natural water bodies.[1,2] Among these pollutants, cationic dyes are particularly relevant due to their high water solubility and strong interactions with biological and environmental surfaces. Basic Blue 41 (BB41), a cationic azo dye containing a positively charged benzothiazolium moiety, is therefore a relevant model pollutant for evaluating the efficiency of novel adsorbent materials.[3]

Several methods have been investigated for dye removal, including coagulation–flocculation, membrane filtration, oxidation, biological treatment, and adsorption. Among these approaches, adsorption has attracted considerable attention due to its operational simplicity, relatively low energy requirements, and potential cost-effectiveness, particularly when renewable materials and industrial by-products are employed.[2,4] Lignocellulosic materials are promising candidates due to their abundance, biodegradability, and surface functionalities capable of interacting with dye molecules through electrostatic attraction, hydrogen bonding, and other intermolecular interactions.[4]

Cellulose, the most abundant natural biopolymer, is particularly attractive for environmental applications due to its renewability, biodegradability, biocompatibility, and abundance of hydroxyl groups.[5] Microcrystalline cellulose (MCC), obtained through the controlled hydrolysis of cellulose-rich materials, combines relatively high crystallinity with a hydroxyl-rich surface, providing a suitable structural support for functional modifications.[6,7] Previous studies have demonstrated the potential of MCC and its derivatives for removing dyes and heavy metals from aqueous solutions, highlighting the importance of surface functionalization in improving adsorption performance.[6,8] In particular, the incorporation of inorganic nanoparticles into

cellulose matrices can provide additional adsorption sites and modify surface properties, increasing the functional versatility of the resulting composites.[8]

Lignosulfonates (LS), water-soluble anionic derivatives of lignin obtained as by-products of the sulfite pulping process, represent valuable renewable components for the development of functional adsorbents. Their heterogeneous aromatic structure contains hydroxyl, methoxy, carbonyl, ether, and sulfonate groups, providing both hydrophobic domains and negatively charged hydrophilic functionalities.[10,11] These structural features are particularly advantageous for cationic dye removal, as sulfonate and carboxylate groups can promote electrostatic interactions with positively charged dye molecules, while aromatic structures may contribute through hydrophobic and π–π interactions. Hydrogen bonding may also participate in dye retention, depending on the solution conditions and material composition.[10–12]

Beyond its potential contribution to dye adsorption, lignosulfonate is particularly interesting for the green synthesis of metallic nanoparticles. Its phenolic hydroxyl groups and other redox-active functionalities may participate in metal-ion reduction, while its macromolecular structure provides dispersing and stabilizing effects, limiting nanoparticle aggregation. Milczarek *et al.*[13] demonstrated the one-step aqueous synthesis of lignosulfonate-stabilized silver nanoparticles (AgNPs), highlighting the dual reducing and stabilizing functions of LS. Modrzejewska-Sikorska *et al.*[14] further showed that nanoparticle formation and characteristics depend on the lignosulfonate type and silver precursor. More recently, lignosulfonate has been investigated as a multifunctional regulator in the mediated synthesis of Ag@AgCl nanocubes, influencing nanoparticle formation and growth.[15] Its reducing and stabilizing capabilities have also been demonstrated in the synthesis of gold nanoparticles,[16] whereas sodium lignosulfonate has been employed as a stabilizing and dispersing agent for ZnO nanoparticles, influencing their dispersion and surface properties.[17] These findings demonstrate the versatility of LS as a bio-based component in the preparation of functional nanostructured materials.

Titanium dioxide (TiO_2) is another relevant inorganic component due to its chemical stability, availability, relatively low cost, and well-established applications in functional materials. It occurs in several crystalline polymorphs, including anatase, rutile, and brookite, with rutile representing the thermodynamically stable bulk phase.[18] Its surface contains hydroxyl groups and coordinatively unsaturated titanium sites, whose protonation and deprotonation are strongly influenced by solution pH. These surface functionalities can participate in interactions with dissolved pollutants, making TiO_2 a potential component of adsorbent materials. Previous theoretical investigations have demonstrated the interaction of cationic methylene blue with rutile and brookite surfaces, emphasizing the importance of surface structure and adsorption-site characteristics.[19] Furthermore, combined theoretical and experimental investigations have confirmed the potential of TiO_2 surfaces to interact with cationic dye molecules in aqueous media.[20] Such interactions provide a basis for exploring TiO_2-containing materials for dye retention, independently of their photocatalytic properties.

The combination of silver and titanium dioxide nanoparticles (Ag/TiO_2) offers further opportunities for tailoring the surface characteristics of hybrid adsorbents. Their incorporation into polymeric or biomass-derived matrices can modify surface composition, particle distribution, and the availability of interfacial adsorption sites. For example, Obayomi *et al.*[9] investigated methylene blue removal using nanoparticle-modified activated carbon derived from coconut shells, demonstrating the potential of combining inorganic nanostructures with a porous carbonaceous support. Similarly, Taha *et al.*[21] developed an Arabic gum-based hydrogel containing Ag/TiO_2 nanoparticles and reported a maximum methylene blue adsorption capacity of approximately 104.5 mg/g under optimized conditions. These studies support the potential of Ag/TiO_2-containing hybrid materials for dye removal through adsorption processes.

Despite these advances, the integration of microcrystalline cellulose, lignosulfonate, TiO_2, and silver nanoparticles into a single hybrid system remains an interesting approach for developing multifunctional adsorbents. In such a system, MCC provides a renewable structural matrix, LS contributes negatively charged functional groups and nanoparticle stabilization, TiO_2 introduces additional inorganic surface sites, while AgNPs act as a complementary surface-modifying component. The combined effects of these constituents may influence the distribution and accessibility of adsorption sites and, consequently,

the interaction of the materials with cationic dye molecules.

Accordingly, the present study investigates the preparation and characterization of lignosulfonate-containing MCC hybrid materials incorporating TiO_2 and AgNPs, with particular emphasis on their application for Basic Blue 41 removal from aqueous solutions. The adsorption performance of the prepared materials is comparatively evaluated against unmodified MCC to establish the contribution of the incorporated functional components. The relationship between the structural and surface properties of the supramolecular architecture and their performance in BB41 removal is also investigated. By combining a renewable cellulose-based matrix with lignosulfonate-mediated silver nanoparticle synthesis and a rutile TiO_2 phase, this work aims to contribute to the development of organic–inorganic hybrid adsorbents for the removal of cationic dyes from contaminated water.

EXPERIMENTAL

Materials

Silver nitrate ($AgNO_3$; 99%), titanium (IV) oxide, rutile (TiO_2NPs; 99.5%; <100 nm particle size), microcrystalline cellulose for thin-layer chromatography, Basic Blue 41 (BB-41; 40% dye content) were purchased from Sigma-Aldrich, and sodium lignosulfonate (LS) – from Carl Roth (Karlsruhe, Germany). NaLS was provided under the form of a fine, homogeneous brown powder (>93% dry substance) with good water solubility, a molecular weight of 18100 g/mol and a polydispersity index of 2.225. All materials were used as received, without any further purification. Ultrapure deionized water was used in all instances.

Preparation of hybrid materials

Preparation of MCC_LS_TiO_2_AgNPs hybrid material

The MCC_LS_TiO_2_AgNPs hybrid material was prepared through a multistep procedure (Fig. 1), as described below.

Stage 1: Preparation of the AgNPs - LS system

The procedure of synthesis was adapted from our previous works.[22,23] Briefly, 0.75 g of LS were added under magnetic stirring (200 rpm) to 50 mL of distilled water in a glass beaker until complete dissolution, the resulting solution showing a non-turbid, yellow-brownish coloration. 15 mg of $AgNO_3$ were dissolved in 5 mL of distilled water in a separate flask and subsequently added dropwise to the lignosulfonate solution under vigorous stirring (1000 rpm). The reduction process was activated by heating the aqueous mixture at 70 °C for 60 min under continuous stirring. A fast increase in the color intensity, resulting in a darker brown/reddish appearance, indicates the formation of silver nanoparticles stabilized by lignosulfonate. The resulting suspensions were allowed to cool to room temperature before using them in the next synthesis stage.

Stage 2: Incorporation of the TiO_2 nano powder

A quantity of 0.25 g of TiO_2NPs was added to the previously obtained suspension. The resulting mixture was subjected to ultrasonication for 60 min in order to promote the disintegration of TiO_2NPs agglomerates, the increase of the contact surface area and thus facilitate the adsorption of the AgNPs - LS system onto the TiO_2 surface.

Stage 3: Incorporation of the cellulose matrix (MCC)

5 g of microcrystalline cellulose were initially hydrated with 50 mL distilled water in a glass beaker and stirred for 10 min. Subsequently, the hybrid suspension obtained in Stage 2 was added to the cellulose suspension. The resulting system was maintained under continuous magnetic stirring for 3 h at room temperature. During this process, the hydroxyl groups of cellulose interact through hydrogen bonding with the lignosulfonate carrying the TiO_2/Ag nanoparticles, thereby promoting their embedding within the cellulose matrix.

Stage 4: Isolation and drying of the MCC_LS_TiO_2_AgNPs material

A solid product was separated from the suspension from Stage 3 by vacuum filtration using a Büchner funnel. The collected material was washed three times with distilled water to remove excess reactants and nanoparticles that had not been effectively retained by the cellulose matrix.

The resulting composite-type material was dried in an oven at 60 °C for 24 h, until constant mass was achieved. The dried material was subsequently ground using a mortar to obtain a fine, homogeneous powder, which was protected from light in a brown glass vessel and stored at room temperature until further characterization and testing.

Preparation of MCC_LS_TiO_2 hybrid material

The MCC_LS_TiO_2 hybrid system was prepared following the same experimental procedure described for the fabrication of MCC_LS_TiO_2_AgNPs, except a modification of Stage 1. Specifically, Stage 1 was completed after the preparation of the sodium lignosulfonate solution, thus excluding the presence of silver species. The quantities and mass ratios of the remaining components were maintained throughout the preparation procedure.

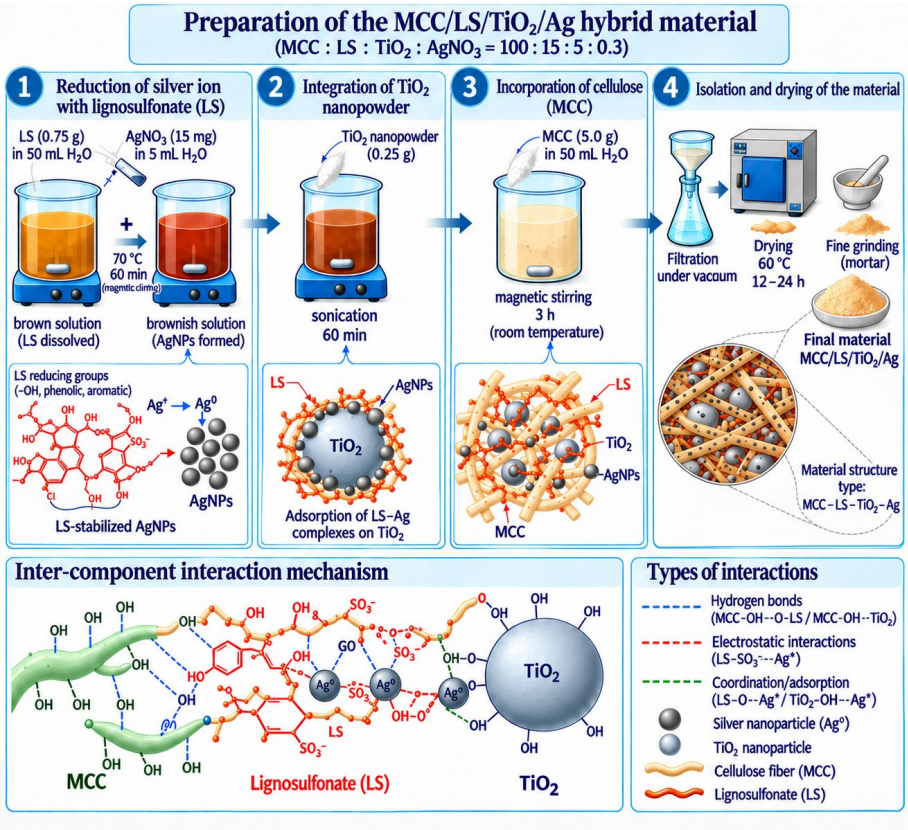


Figure 1: Preparation process of hybrid materials and inter-component interactions

Preparation of the MCC_LS_AgNPs hybrid material

The MCC_LS_AgNPs hybrid system was prepared following the experimental procedure established for MCC_LS_TiO_2_AgNPs, with Stage 2 omitted. Consequently, the step involving the incorporation of TiO_2 was excluded. The quantities and mass ratios of the remaining components were maintained throughout the preparation procedure.

Characterization

Fourier-transform infrared (FTIR) spectra were recorded on a Bruker Vertex 70 FTIR spectrometer equipped with an attenuated total reflectance (ATR) accessory fitted with a ZnSe crystal. Measurements were performed over the wavenumber range of 4000–400 cm^{-1}, using 64 scans per spectrum, a spectral resolution of 2 cm^{-1}, and an incidence angle of 45°.

The UV–Vis spectra of dye solutions were recorded on a Lambda 35 UV–Vis spectrophotometer (PerkinElmer), by using standard 1 cm path-length quartz cuvettes. The maximum absorption wavelength ($\lambda\, max$) was determined to be 611 nm, and this wavelength was subsequently used for monitoring dye concentrations during the adsorption experiments.

Powder X-ray diffraction (XRD) analysis was performed using a Rigaku SmartLab diffractometer (Tokyo, Japan) equipped with a Cu anode (Cu Kα radiation, λ = 1.5406 Å). The instrument was operated at a tube voltage of 45 kV and a current of 200 mA. The crystalline phases present in the samples were identified by comparing the experimental diffraction patterns with reference data available in the Crystallography Open Database (COD).

Polarized light microscopy images for morphological analysis were acquired at room temperature by a polarized optical microscopy (POM) using a Zeiss Axio Imager.A2m microscope equipped with 10×, 20×, and 50× objectives, crossed polarizers, and a rotatable 530 nm λ retardation plate oriented at 90° (black background). Furthermore, both morphological characteristics and elemental mapping were investigated by using a Quanta 200 scanning electron microscope (FEI Company), equipped with an energy-dispersive X-ray spectroscopy (EDX) system (EDAX silicon drift detector).

Basic Blue 41 cationic dye retention by materials

The retention performance of the MCC_LS_TiO_2_AgNPs, MCC_LS_TiO_2, and MCC_LS_AgNPs hybrid composites, as well as that of the raw MCC, has been investigated using a batch adsorption technique. Dye retention capacity (q_t) and

removal efficiency (R) were calculated according to the following equations:

$$q_t = \frac{(C_0 - C_t)V}{m}; \text{(mg/g)} \quad (1)$$

$$R = \frac{(C_0 - C_t)100}{C_0}; (\%) \quad (2)$$

where (C_0) and (C_t) represent the initial dye concentration, respective the residual dye concentration (mg/L) at time (t), (V) is the volume of dye solution (L), and (m) is the mass of the adsorbent (g).

For each experiment, 100 mg of powder were added to 80 mL of BB 41 aqueous solution (100 mg/L) in an Erlenmeyer flask. The adsorption tests were conducted at room temperature (20±2°C), under continuous magnetic stirring at 250 rpm. Aliquots of 2 mL were collected at predetermined contact times of 10, 20, 30, 45, 60, 90, 120, 180, 240, and 300 min. Before each sampling, stirring was stopped for 1 min to allow the solid particles to settle, and the supernatant was carefully collected.

All collected samples were centrifuged at 6000 rpm for 4 min to ensure the effective separation of residual materials particles from the liquid phase. The absorbance of the resulting supernatants, corresponding to the residual BB 41 concentration, was then measured on the UV-Vis spectrophotometer at 611 nm wavelength. The residual dye concentrations (C_t) were determined using an appropriate calibration curve. All adsorption experiments were performed under identical experimental conditions to ensure the comparability of the results.

RESULTS AND DISCUSSION

Composition and component ratios

The selection of composition and component ratios has been made following the analysis of several convergent data from our previous works and other reports. First of all, crystalline celluloses can provide the main structural framework of a composite, while LS acts as a multifunctional component, cooperatively contributing to the reduction, stabilization, and dispersion of AgNPs.[14,23,24] While MCC may be effective in adsorption through the synergistic effect of hydrogen bonding and van der Waals interactions rather than due to the electrostatic attraction of positively charged compounds,[25] the TiO_2NPs and AgNPs are the active components that could promote processes of dye degradation. TiO_2NPs serve as the primary active component, whereas AgNPs play the role of a surface modifier and electron-trapping agent, which potentially enhances charge separation and inhibits electron-hole recombination through the formation of a metal-semiconductor interface.[26,27] Nevertheless, excessive silver depositions may block active sites and hinder light penetration, ultimately compromising the TiO_2 photocatalytic performance.[26,27] Therefore, a relatively low silver loading was selected to promote the beneficial effects of silver, without excessively covering the TiO_2 surface, namely, an amount of around 5-6 wt% of the nitrate precursor. Taking into account loses occurring during nanoparticle formation, such a loading is typical of a dopant.

On the other hand, an insufficient LS amount may favor nanoparticle aggregation, thereby compromising their dispersion and functional efficiency, while an excessive quantity may result in the materials browning and increased light absorption by the lignosulfonate itself, which may further conduct to an UV-screening effect, limiting light penetration and potentially influencing the performance of TiO_2 NPs.[26,28] Consequently, the LS content should vary within the range of 10–20 wt% relative to MCC for promoting the effective stabilization and distribution of an appropriate amount of AgNPs.

Based on these considerations, the overall mass ratio calculated on a dry-mass basis for the raw materials used to prepare the hybrid material, MCC:LS:TiO_2:$AgNO_3$, has been established at 100:15:5:0.3.

FTIR analysis and interfacial interactions in MCC–LS–TiO_2–AgNPs materials

The FTIR spectra of the prepared composites (Fig. 2a) exhibit almost similar profiles, which was largely expected due to the major content in MCC (about 80-85 wt%). The recorded spectra also suggest that the main structural features of cellulose matrices are retained following the incorporation of the inorganic components, whereas the characteristic lignosulfonate footprint absorbances became indiscernible, probably due to both masking and extensive interactions with the other materialscomponents. The major absorption bands identified in the materialsspectra are located at approximately 3348, 2902, 1643, 1426, 1370, 1329, 1167, 1113, 1059, 1025, 893, 667, 608, 559, and 510 cm^{-1}, corresponding to the pure MCC spectrum, with negligible deviations of less than 3 nm.

A broad absorption band centered at 3348 cm^{-1} is primarily attributed to O–H stretching vibrations of the hydroxyl groups present in MCC and LS, as well as to those associated with adsorbed water molecules. The corresponding spectra of the starting compounds (Fig. 2b) also exhibit broad absorption features in this region, confirming the contribution of hydroxyl-containing structures to

absorbance pattern of hybrid products. The persistence of this band at nearly the same wavenumber in all three materials suggests that the hydroxyl groups remain an important structural feature. Nevertheless, changes in the local hydrogen-bonding environment may occur during materialsformation.[29,30] The absorption band from approximately 2902 cm^{-1} corresponds to the aliphatic C–H stretching vibrations associated with the polysaccharide backbone of cellulose, which overlay the 2931 cm^{-1} weaker absorbance generated by minor non-aromatic lignosulfonate structures.[29,31]

The 1643 cm^{-1} band is usually assigned to the H–O–H bending vibration of physically adsorbed water. This assignment is consistent with the hygroscopic character of cellulose-based materials and the presence of hydroxyl-rich surfaces.[29,30] Although LS contains aromatic structures that should contribute to the spectral profile at around 1600 cm^{-1}, the only perceptible trace is given by a 2-3 nm shift of absorbance maxima, from 1645-1646 cm^{-1} at pure MCC to 1643 cm^{-1} in resulting materials, without changes in intensity or width. A possible explanation is related to the π-π interactions potentially established between aromatic, phenolic, and metallic moieties. The LS characteristic aromatic skeletal vibrations combined with C=O stretching from 1510 cm^{-1} are also virtually missing in composites, despite a lesser potential overlap with MCC absorbances, which may further confirm strong interactions with the surface of associated metallic nanoparticles. CH_2 and C-H bending vibrations from methylene and methyl groups are responsible for 1426 cm^{-1} and 1370 cm^{-1} absorbance peaks, while the 1329 cm^{-1} one may be assigned to CH_2 wagging and O–H in-plane bending vibrations of both cellulose and lignosulfonate moieties.[29-32]

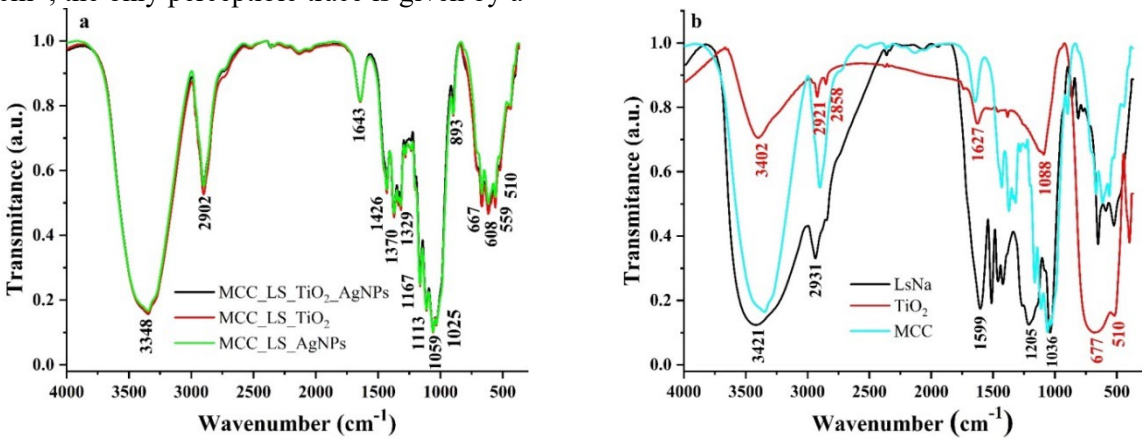


Figure 2: FTIR spectra of MCC_LS_TiO_2_AgNPs, MCC_LS_TiO_2, MCC_LS_AgNPs hybrid materials (a), and respectively LS, TiO_2 and MCC raw compounds (b)

Overlapping vibrational contributions from both MCC and LS oxygen-containing functional groups mostly contribute to the spectral profile between 1200 and 1000 cm^{-1}, with the 1167 cm^{-1} band primarily associated with C–O–C stretching vibrations of the β-(1,4)-glycosidic linkages and the 1113, 1059, and 1025 cm^{-1} ones with C–O and C–O–C stretching vibrations. The LS contributions, including the sulfonate stretching vibrations from this region, are copiously overlayed by the strong MCC absorbances.[31,32] The absorption band from 893 cm^{-1} is characteristic of celluloses and is related to the vibrations of β-glycosidic linkages that connect the glucose units. Its presence in the spectra of all three hybrids indicates that the integrity of the main polysaccharide framework is preserved during the preparation process.[29,30]

In the lower wavenumber region, the absorption bands observed at around 667, 608, 559, and 510 cm^{-1} originate from the overlapping contributions of organic and inorganic constituents. The reference spectrum of TiO_2 exhibits a pronounced absorption in the 800-500 cm^{-1} region, which is characteristic of Ti-O and Ti-O-Ti lattice vibrations. Consequently, the slight increases in absorbance intensity in this region exhibited by the TiO_2-containing materials are consistent with the incorporation of TiO_2 phases.[33,34] Nevertheless, some of these absorptions may also contain vibrations associated with sulfonate groups and other deformation modes of the organic matrices.

A comparative analysis of all materials spectra reveals that TiO_2NPs and AgNPs does not substantially alter the main absorption bands associated with the MCC matrix. However, minor differences in band intensity and shape, particularly in the regions between 1500 and 1000 cm^{-1} and below 800 cm^{-1}, indicate changes in the spectral contributions of the organic and inorganic constituents. These variations may reflect modifications in the local chemical environment and interfacial interactions established during materials formation. In particular, hydrogen bonding between hydroxyl-containing groups of MCC and oxygen-containing surface sites, together with adsorptive and coordinative interactions involving aromatic and functional groups of LS and inorganic particles, may contribute to the stabilization of hybrid structure.[33,34]

Overall, these results indicate that the characteristic structural features of MCC are largely preserved in the synthesized composites, while the absorption features in the low-wavenumber region are consistent with the presence of inorganic TiO_2 phase. The spectral similarities among composites further suggest that LS matrices are strongly involved in various interactions with MCC and metallic components, but the relatively low proportion does not provide enough evidence to establish the exact nature of these interactions. Moreover, the concentration of AgNPs is well beyond the detection limit to have a direct confirmation of their presence.

Interaction mechanisms within MCC–LS–TiO_2–AgNPs hybrid materials

The proposed interaction mechanism within the MCC–LS–TiO_2–AgNPs hybrid materials relies on the complementary roles of its individual constituents and interfacial interactions established between the organic and inorganic phases. MCC provides the main structural framework of the composite, owing to its polysaccharide backbone, abundance of hydroxyl groups that could participate in hydrogen-bonding interactions, and high compositional extent. On the other hand, LS, characterized by a phenylpropanoid structure and various oxygen-containing functional groups, mainly phenol and sulfonate, plays a multifunctional role in the materials formation process. Well-known as a traditional binder and surfactant agent, LS acts as a both reducing and stabilizing agent during the green synthesis of AgNPs. Its reducing capacity facilitates the conversion of Ag^+ ions into metallic silver (Ag^0), while its functional groups contribute to the stabilization of resulting AgNPs, limiting their aggregation and promoting their dispersion within the materialsmatrix.[13,14,35] Furthermore, the ability of lignosulfonates to interact with metal ions through π-π interactions and complexation processes also contribute to the formation and stabilization of LS-associated AgNPs.[13,14]

The incorporation of TiO_2NPs into MCC_LS matrices is expected to involve interfacial interactions between the hydroxylated TiO_2 surface and the functional groups of the organic counterparts. Similar connections have been reported in cellulose/TiO_2 hybrid systems, where infrared spectral modifications have been associated with interfacial interactions between cellulose chains and TiO_2NPs.[36,37] LS-associated AgNPs are envisaged to distribute and stabilize throughout the MCC matrix, and correspondingly at the surface of TiO_2NPs, which may behave as a matrix reinforcement and as the main inorganic photoactive phase. The coexistence of these components is highly conducive to the formation of a hybrid network stabilized by coordinative and multiple weak non-covalent interactions like hydrogen bonding, electrostatic, and van der Waals interactions, which all together enhance the compatibility and structural stability of the analysed systems.[38] Since infrared spectroscopy alone cannot assist in establishing the exact nature, type and spreading of interactions within the prepared materials, complementary characterization techniques were carried out.

The crystalline structure of raw materials and synthesized hybrid materials was investigated by powder X-ray diffraction (XRD) (Fig. 3). The diffraction pattern of MCC exhibits characteristic reflections at about 15-17° and 22-23° (2θ), which are consistent with the semicrystalline structure of cellulose (Fig. 3b). Furthermore, the reflection located around 22.6° (2θ) is commonly associated with the (200) crystallographic plane, whereas the reflections from the 14.8-16.5° (2θ) region arise from other crystallographic planes of the cellulose structure.[39,40] In contrast, LS displays a broad diffraction profile, without well-defined intense reflections, confirming its predominantly amorphous character.

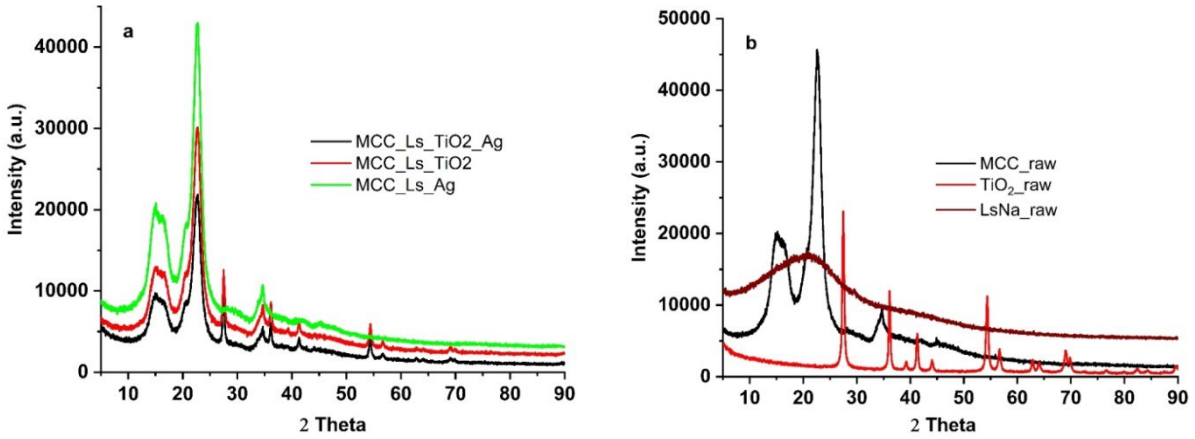


Figure 3: X-ray diffraction patterns of hybrid materials and initial precursors

The analysis confirmed that the TiO_2 precursor is composed of a single crystallographic phase, namely Tetragonal Rutile (COD entry no. 9004142). The crystallographic structure of the MCC matrix suffered no detectable modification following the introduction of TiO_2NPs and AgNPs (Fig. 3). In TiO_2-containing materials, the rutile 110, 101, 111, 120, 211, 220, 002, 130, 301 and 112 reflections are visible at approximately 27.4, 36.1, 41.2, 54.3, 56.6, 62.8, 64.1, 69.0, and 69.8° (2θ) respectively.[41,42]

The diffraction patterns of all materials retain the main reflections associated with MCC unchanged, respectively, those located in the 15-17, 22-23, and 34-35° (2θ) regions. So, the semicrystalline structure of cellulose matrices is essentially preserved during materials' preparation. The rutile TiO_2 crystalline phase was also maintained after incorporation, the main reflections being preserved without pattern modifications. Unfortunately, the diffraction patterns do not provide an unequivocal set of reflections attributable to metallic silver. The characteristic reflections for face-centered cubic (fcc) metallic silver are generally observed at 38.1°, 44.3°, 64.4°, and 77.4° (2θ), corresponding to the (111), (200), (220), and (311) crystallographic planes, respectively.[43,44] Silver specific reflections are not sufficiently distinct from the noise background to confirm its presence. The overlap with reflections from other crystalline phases may play a modest role, the main issue being clearly the very low amount existing in the analyzed sample, below the limit of detection of this technique.

The results obtained by X-ray diffraction are consistent with the infrared findings regarding the preservation of cellulosic crystalline moieties, subtle changes taking place mainly within the microlocal environment of oxygen-containing functional groups associated with interfacial interactions between system components. Such interactions have also been reported for cellulose/TiO_2 hybrid systems.[36,37]

Morphological considerations of hybrid materials

Interfacial interactions between system components conduct to aggregate formation during hybrid materials preparations, as obviously shown by the POM micrographs of MCC and its derived composites with LS, TiO_2NPs, and AgNPs (Fig. 4).

There are notable differences in particle morphology, aggregation behavior and optical anisotropy following the incorporation of LS, TiO_2NPs, and AgNPs into the cellulose matrix. As regards the approximate sizes of particles involved, it should be noted that, while synthesized AgNPs are mostly within the 20-40 nm range, TiO_2NPs go up to 100 nm, while pristine MCC is at least one order of magnitude larger and may even exceed 10 μm in size. The birefringent optical response observed in all four samples indicates that optically anisotropic domains remain effective after hybrid materials preparation. This is particularly relevant, since MCC is a semicrystalline polymer, whose ordered molecular and microfibrillar organization contributes to its birefringent properties. Changes in optical texture and brightness can therefore provide qualitative information about the distribution and orientation of cellulose-rich domains.[45-47]

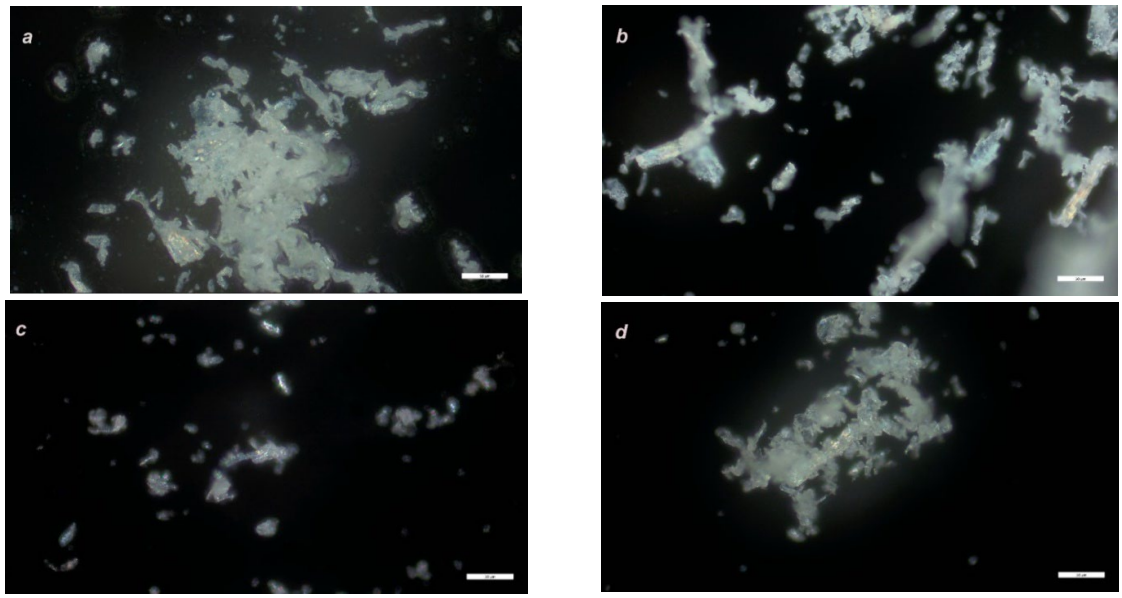


Figure 4: POM micrographs of: (a) MCC_LS_TiO_2_AgNPs, (b) MCC_LS_TiO_2, (c) MCC_LS_AgNPs, and (d) pristine MCC (scale bars: 50 μm)

The addition of LS and inorganic components to MCC strongly influences the particle aggregation behavior. In particular, the significant increase in the disperse appearance of MCC_LS_AgNPs, as compared to pristine MCC, in the case of low metal content, demonstrates the efficient dispersive effect of LS (Fig. 4c, d). When higher amounts of bulkier TiO_2NPs are involved (Fig. 4b), the dispersive effect of LS became rather elusive, and a tendency for ordered, cumulative short-bar structures typical of MCC is quite obvious. Finally, despite the very low amount of AgNPs, the simultaneous incorporation of TiO_2NPs contributes to the formation of larger micrometric aggregates, which also seem to contain combined bar-like structures and appear more like a loose, intertwined hybrid systems (Fig. 4a). These observations are highly consistent with the assumption of strong overall interactions between the hydroxyl-rich cellulose matrix, lignosulfonate functional groups, and inorganic components.

The most substantial details and evidence regarding the morphological aspect of hybrid systems are given by the SEM/EDX images, which fully confirm the presence, sizes and surface characteristics of all components and prove their successful preparation (Figs. 7-9). The images for commercial raw materials (MCC and TiO_2) were additionally presented for comparison (Figs. 5-6).

The increased surface area through the substantial roughness induced to the relatively flat, exfoliating-like MCC surface by the insertion of inorganic particles is a clear advantage for dye retention. It further appears that the presence of LS had itself a subtle effect on the nanometric patterns on the MCC surface, while the small, elusive AgNPs could be finally observed (Figs. 5b, 7b).

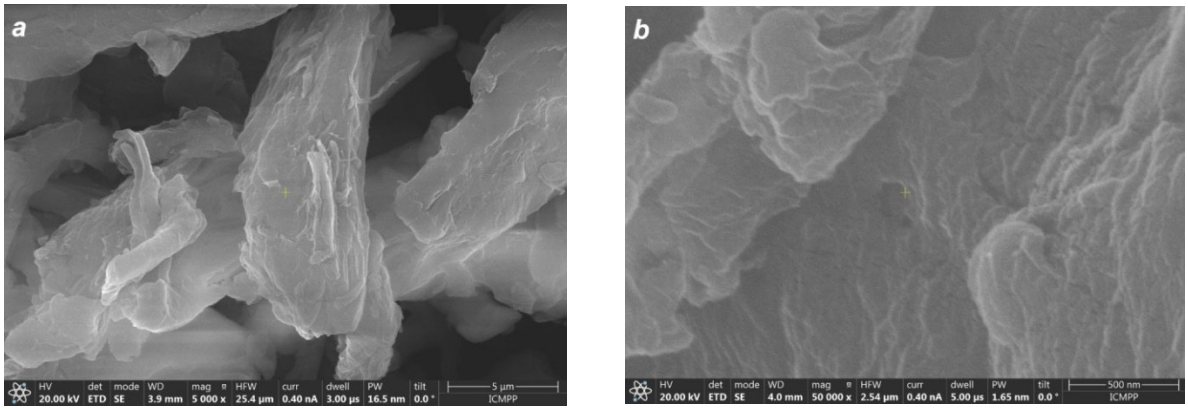


Figure 5: SEM micrographs of raw MCC at magnifications of: a) 5000x and b) 50000x

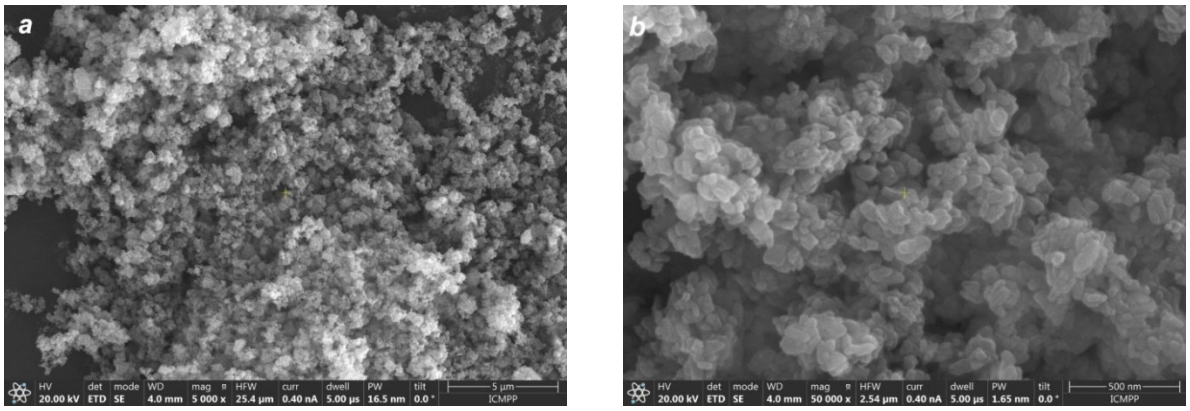


Figure 6: SEM micrographs of raw TiO_2 at magnifications of: a) 5000x and b) 50000x

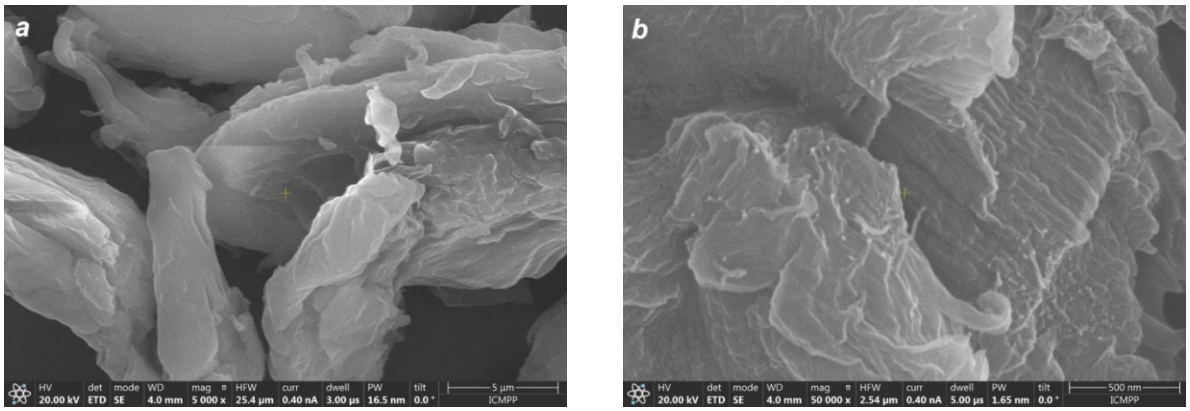


Figure 7: SEM micrographs of MCC_LS_AgNPs at magnifications of: a) 5000x and b) 50000x

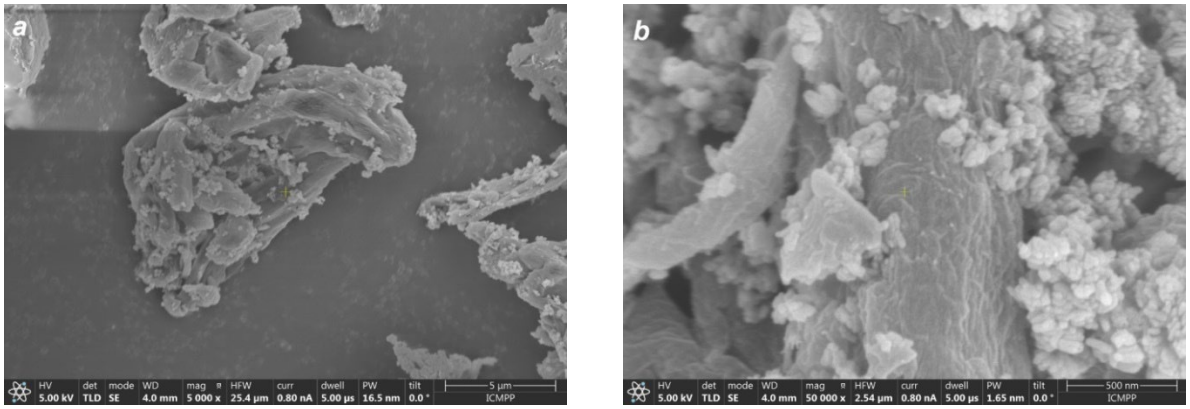


Figure 8: SEM micrographs of MCC_LS_TiO_2 at magnifications of: a) 5000x and b) 50000x

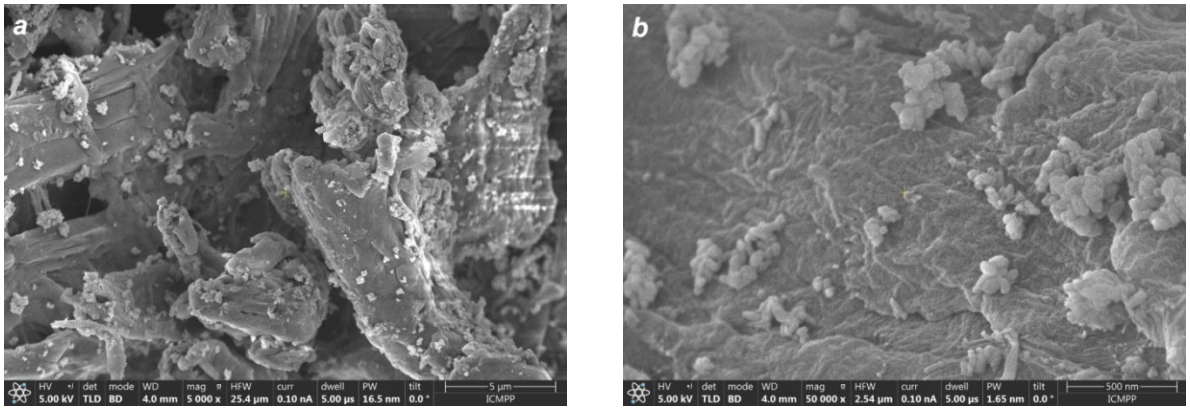


Figure 9: SEM micrographs of MCC_LS_TiO_2_AgNPs magnified at: a) 5000x and b) 50000x

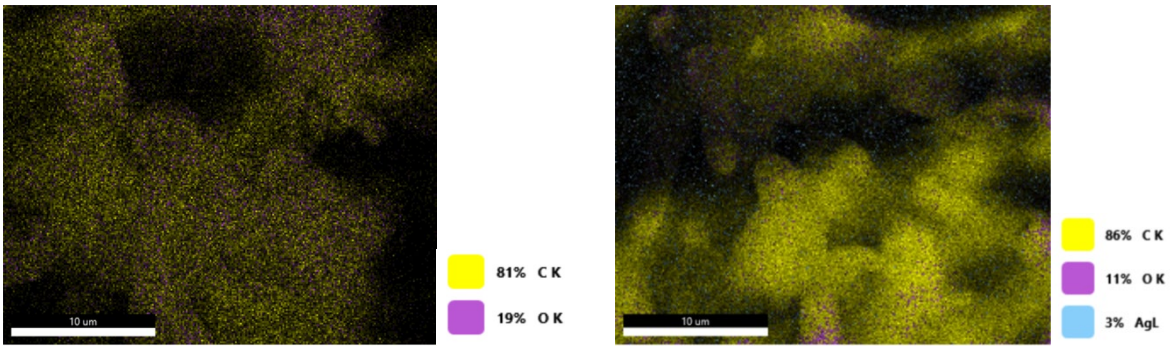


Figure 10: EDX mapping of MCC (left) and MCC_LS _AgNPs (right) elemental composition

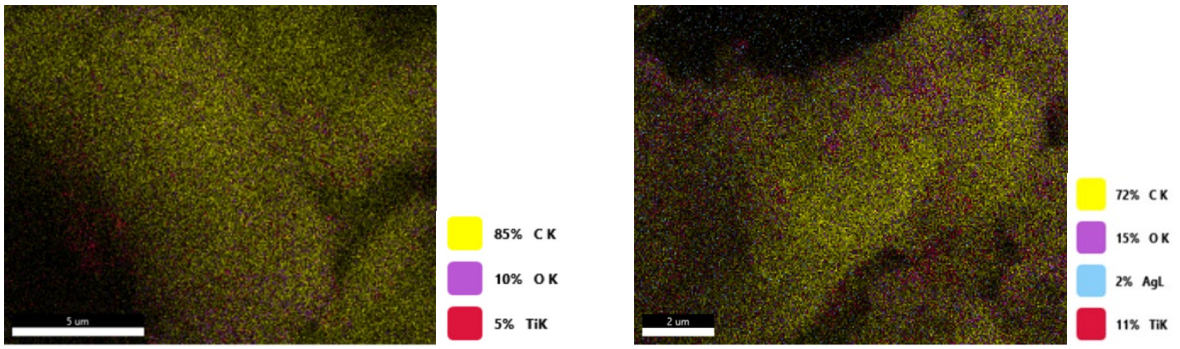


Figure 11: EDX mapping of MCC_LS_TiO_2 (left) and MCC_LS_TiO_2_AgNPs (right) elemental composition

EDX mapping of random features from samples observed by SEM reveals a quite good dispersion of metallic components and elemental compositions in good agreement with the other experimental data previously described (Figs. 10, 11). A more detailed EDX mapping analysis of the hybrid materials (of sequential elements) is further shown in Figure 12; whereas the values obtained as a median of 5 measurements of each hybrid system are included within Table 1.

The EDX elemental maps (Fig. 12) and EDX elemental analysis (Table 1) reveal the presence of carbon (C) and oxygen (O) as the predominant elements in all three materials, consistent with the organic nature of the microcrystalline cellulose (MCC) and sodium lignosulfonate (LS) matrix. Their spatial distributions indicate that these elements are present throughout the analyzed regions, confirming the continuity of the carbonaceous biopolymer-based matrix.

For the MCC_LS_TiO_2 sample, titanium (Ti) was detected with a weight concentration of 1.96% and an atomic concentration of 0.56%. The corresponding elemental mapping confirms the presence of Ti across the analyzed area, supporting the successful incorporation of TiO_2 into the MCC/LS matrix. The relatively dispersed distribution of the Ti signal suggests that the titanium-containing phase is distributed within the polymeric matrix, although some local variations in signal intensity can be observed.

In the MCC_LS_AgNPs, the presence of silver (Ag) was confirmed by the characteristic Ag L signal, with a measured concentration of 0.104 wt% and 0.014 at%. The Ag elemental map indicates a spatially distributed signal throughout the investigated region, suggesting the incorporation of silver-containing nanoparticles into the MCC/LS matrix. The low silver concentration is consistent with the relatively small amount of silver precursor used during the synthesis.

The ternary MCC_LS_TiO_2_AgNPs system exhibits the characteristic signals of all four elements (C, O, Ti, and Ag), confirming the simultaneous incorporation of both inorganic components into the MCC/LS matrix. The measured Ti and Ag concentrations were 2.96 wt% and 0.09 wt%, respectively. The elemental maps demonstrate the coexistence of the Ti- and Ag-containing phases within the same analyzed region. Although variations in local signal intensity are visible, both elements are detected across the investigated area.

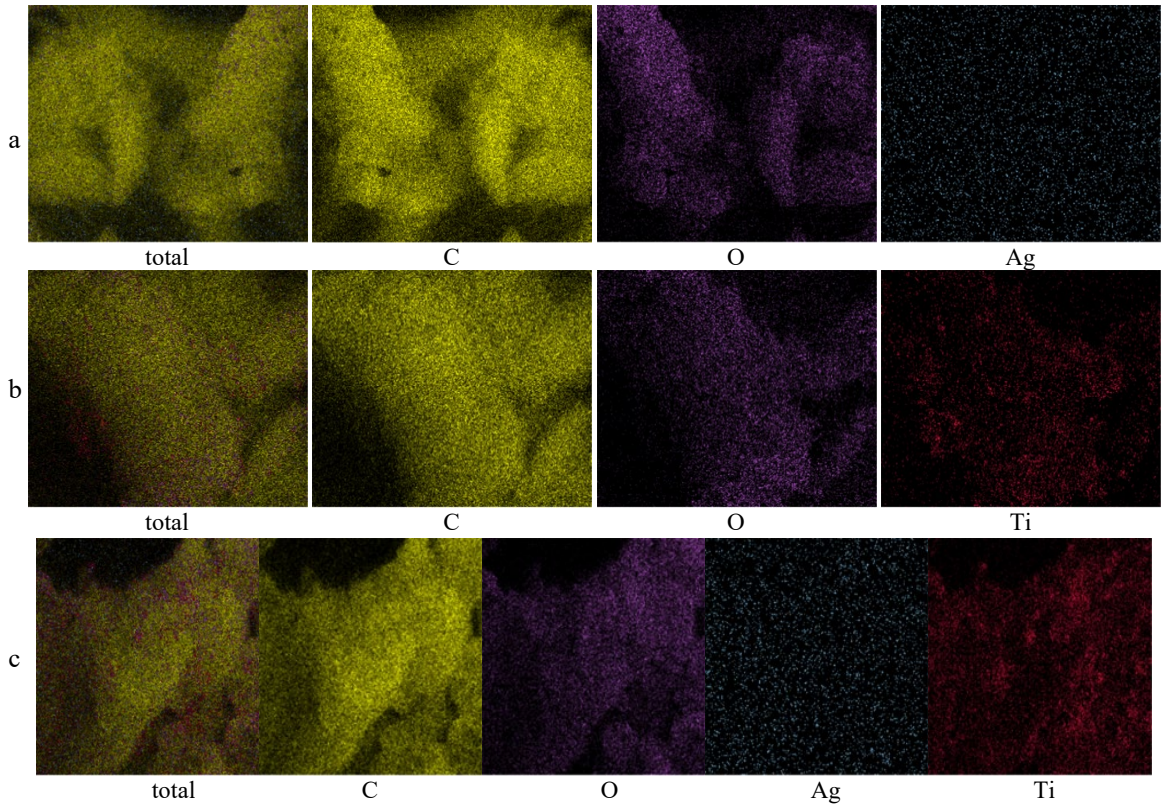


Figure 12: EDX sequential mapping of individual elements for: a) MCC_LS_AgNPs; b) MCC_LS_TiO_2; c) MCC_LS_TiO_2_AgNPs

Table 1
EDX elemental analysis of hybrid systems

Sample	MCC_LS_TiO_2_AgNPs		MCC_LS_TiO_2		MCC_LS_AgNPs	
element	weight %	atomic %	weight %	atomic %	weight %	atomic %
C K	69.18	79.41	70.78	79.76	74.34	81.80
O K	22.41	19.34	22.91	19,38	21.69	17.92
TiK	2.96	0.86	1.96	0.56	-	-
AgL	0.09	0.012	-	-	0.104	0.014

A comparison of the three samples indicates that the incorporation of TiO_2 and AgNPs does not substantially alter the predominance of carbon and oxygen in the materials structure. The simultaneous detection of Ti and Ag in MCC_LS_TiO_2_AgNPs provides evidence for the successful formation of the hybrid material containing both inorganic components within the biopolymer-based matrix.

Overall, the EDX results, together with the corresponding elemental distribution maps, support the successful preparation of the MCC_LS_TiO_2_AgNPs. These findings provide complementary evidence for the incorporation of the inorganic phases into the cellulose–lignosulfonate matrix.

Basic Blue 41 removal by hybrid materials

The activation of MCC by embedding LS, TiO_2NPs, and AgNPs was tested for the removal of a model cationic dye. The retention of BB41 cationic dye by each hybrid material was investigated as a function of contact time and compared with that of unmodified MCC. The adsorption capacity (qt, mg/g) and corresponding dye removal efficiency (R, %) are presented in Figure 13 (a, b), while the visual appearance of treated solutions is shown in Figure 13 (c).

All investigated materials exhibit a similar time-dependent retention profile (Fig. 13 a, b) characterized by a rapid initial uptake, followed by a considerably slower, but continuous increase. The most pronounced increase occurs during the first 10 min of contact, suggesting a rapid

interaction of BB41 molecules with the readily accessible adsorption sites on the material surfaces. Thus, after just 10 minutes of contact, the retention values attained 27.4 mg/g for MCC, 37.48 mg/g for MCC_LS_AgNPs, 42.16 mg/g for MCC_LS_TiO_2, and 50.71 mg/g for MCC_LS_TiO_2_AgNPs, while dye removal efficiencies were of 34.48%, 46.99%, 53.22%, and 66.02%, respectively. The faster retention system, MCC_LS_TiO_2_AgNPs, practically retains about 81% within the first 10 minutes from the total time of 300 minutes, while the slowest acting MCC removes approximately 62%. Over time, the adsorption rate decreases, which may be attributed to the progressive occupation of available sites and the increasing contribution of mass transfer towards less accessible regions of the adsorbent structure. The flattening of the curves indicates that the systems tend to enter a region of stabilization. However, a slight increase in both qt and R observed throughout the final part of the tests indicates that adsorption equilibrium could not be reached within the investigated contact time of 300 min.

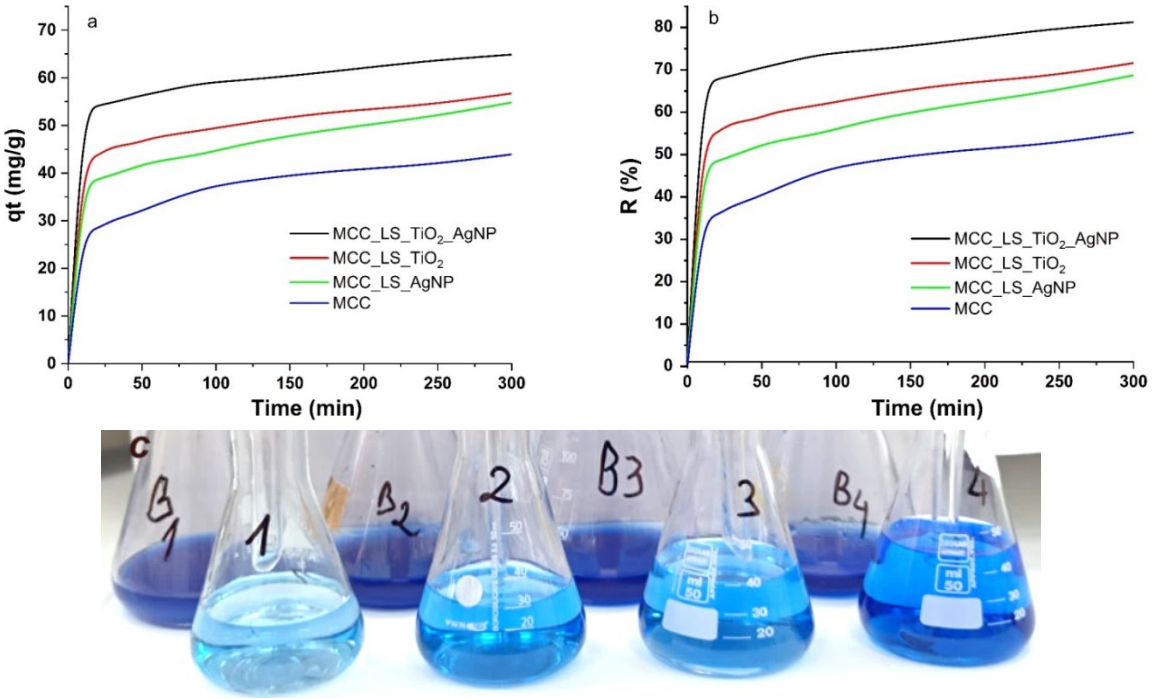


Figure 13: Retention of BB41 over time: (a) adsorption capacity (qt, mg/g); (b) dye removal efficiency (R); and (c) photographs of samples after 300 min treatment (B1-B4), and after subsequent filtration (1-4): 1 – MCC_LS_TiO_2_AgNPs; 2 – MCC_LS_TiO_2; 3 – MCC_LS_AgNPs; 4 – MCC

A comparison of the adsorption capacities after 300 min (Fig. 13a) reveals clear differences between unmodified MCC and functionalized ones. The approximate qt values were 43.93 mg/g for MCC, 54.81 mg/g for MCC_LS_AgNPs, 56.73 mg/g for MCC_LS_TiO_2, and 64.88 mg/g for MCC_LS_TiO_2_AgNPs. The corresponding dye removal efficiencies were of 55.29%, 68.73%, 71.62%, and 81.26%, respectively. Thus, all three hybrid materials exhibited improved BB41 retention, compared with the raw cellulose. These results demonstrate the beneficial effect of modifying the MCC-based matrix with lignosulfonate and inorganic constituents under the investigated experimental conditions.

Among the tested materials, MCC_LS_TiO_2_AgNPs displayed the highest retention performance, reaching an adsorption capacity of 64.88 mg/g and a dye removal efficiency of about 81.26% after 300 min. This capacity is almost 50% higher than that of unmodified MCC. The enhanced performance may be associated with the complementary contribution of the organic and inorganic constituents, which can modify the surface characteristics of the cellulose-based matrix and provide additional sites for interactions with the analyzed dye.

The LS contributions may be particularly relevant due to its sulfonate and hydroxyl functional groups. The negatively charged

sulfonate groups can complement the negatively charged MCC in promoting electrostatic attraction of positively charged BB41 molecules, whereas the hydroxyl groups may participate in hydrogen-bonding interactions. Furthermore, the aromatic LS domains may contribute to the dye retention through interactions with the aromatic structure of BB41, including π–π interactions. Electrostatic and other intermolecular interactions have also been discussed in previous studies on BB41 adsorption by chemically modified lignocellulosic materials.[48]

The incorporation of TiO_2 further improves BB41 retention, which may be related to the presence of additional surface hydroxyl groups and pH-dependent surface charge behavior of TiO_2, which can positively influence its interactions with dye molecules in aqueous media. Likewise, TiO_2NPs seem to impact the cooperative behavior of MCC. The use of TiO_2/calcium alginate beads for BB41 removal has been reported for the combined adsorption and photocatalytic degradation of this dye, confirming the high potential of such composites for both adsorption and photocatalytic degradation.[49] A further increase in retention was observed when AgNPs were incorporated into the MCC_LS_TiO_2 system which, despite the very low amount used, is believed to have a significant influence on the surface and cooperative properties of hybrid material, indirectly enhancing the retention of the dye.

The macroscopic appearance of the treated solutions (Fig. 13c) adds qualitative evidence to the differences observed during spectrophotometric measurements. The treatment with MCC_LS_TiO_2_AgNPs (sample 1) conducts to the most pronounced color decrease, whereas the samples treated with unmodified MCC (sample 4) retain the most intense blue color. The other ones (samples 2, 3) display intermediate coloration. This visual trend agrees with the adsorption capacity and removal efficiency sequence determined experimentally: MCC_LS_TiO_2_AgNPs > MCC_LS_TiO_2 > MCC_LS_AgNPs > MCC.

Overall, these combined results undoubtedly demonstrate the potential of these hybrid materials for the removal of cationic dyes from aqueous solutions. Systems' optimization of MCC embedded AgNPs and TiO_2NPs, including the complementary potential of photocatalytic degradation of the retained dye, are currently underway on series of both cationic and anionic dyes.

CONCLUSION

MCC-based hybrid materials incorporating sodium lignosulfonate, TiO_2, and/or silver nanoparticles were successfully developed and evaluated for the retention of BB41 cationic dye from aqueous solutions. FTIR and XRD analyses indicate that the main structural features of cellulose were preserved after materials preparation, and the rutile phase was retained in TiO_2-containing materials, while POM observations reveal significant changes in particle aggregation following the incorporation of the functional components. SEM/EDX data confirm the successful integration of all components within the final systems, as well as their dimensional characteristics.

All hybrid materials exhibit higher BB41 retention than pristine MCC. After 300 min, MCC_LS_TiO_2_AgNPs achieved the highest adsorption capacity (64.88 mg/g) and removal efficiency (81.26%), compared with 43.93 mg/g and 55.29%, respectively, for pristine MCC. The adsorption capacity of the ternary hybrid was approximately 1.48 times higher than that of MCC. A rapid initial uptake was observed during the first 10 minutes, followed by a slower increase, with no clear evidence that equilibrium had been reached within the investigated period.

The improved retention results arise from cooperative interactions that involve the LS and MCC functional groups, respectively, the surface morphology and functionality of all organic and inorganic components. Overall, these preliminary results validate the potential of combining LS, TiO_2, and silver-based components to enhance the performance of cellulose-based adsorbents for cationic dye removal. Further investigations will be done to evaluate and clarify the adsorption mechanisms, to optimize and expand the potential applicability to wastewater treatments, and to assess the regeneration and reusability parameters of such materials systems.

REFERENCES

[1] J. Lin, W. Ye, M. Xie, D. H. Seo, J. Luo *et al*., *Nat. Rev. Earth Environ*., **4**, 785 (2023), https://doi.org/10.1038/s43017-023-00489-8

[2] R. Al-Tohamy, S. S. Ali, F. Li, K. M. Okasha, Y. A.-G. Mahmoud *et al*., *Ecotoxicol. Environ. Saf*., **231**, 113160 (2022), https://doi.org/10.1016/j.ecoenv.2021.113160

[3] M. Tidjani, A. Dehane, S. Merouani, C. Djelloul and O. Hamdaoui, *Asia-Pacific J. Chem. Eng*., **21**, e70138 (2026), https://doi.org/10.1002/apj.70138

[4] K. Roa, E. Oyarce, A. Boulett, M. Al-Samman, D. Oyarzún *et al*., *Sustain. Mater. Technol*., **29**, e00320 (2021), https://doi.org/10.1016/j.susmat.2021.e00320
[5] D. Klemm, B. Heublein, H.-P. Fink and A. Bohn, *Angew. Chem. Int. Ed*., **44**, 3358 (2005), https://doi.org/10.1002/anie.200460587
[6] Z. N. Garba, I. Lawan, W. Zhou, M. Zhang, L. Wang *et al*., *Sci. Total Environ*., **717**, 135070 (2020), https://doi.org/10.1016/j.scitotenv.2019.135070
[7] U. Hapani and L.-B. George, *Cellulose Chem. Technol*., **60**, 15 (2026), https://doi.org/10.35812/CelluloseChemTechnol.2026.60.02
[8] A. Kausar, S. T. Zohra, S. Ijaz, M. Iqbal, J. Iqbal *et al.*, *Int. J. Biol. Macromol.*, **224**, 1337 (2023), https://doi.org/10.1016/j.ijbiomac.2022.10.220
[9] K. S. Obayomi, S. Y. Lau, A. Zahir, L. Meunier, J. Zhang *et al*., *Chemosphere*, **313**, 137533 (2023), https://doi.org/10.1016/j.chemosphere.2022.137533
[10] J. Ruwoldt, *Surfaces*, **3**, 622 (2020), https://doi.org/10.3390/surfaces3040042
[11] T. Aro and P. Fatehi, *ChemSusChem*, **10**, 1861 (2017), https://doi.org/10.1002/cssc.201700082
[12] T. N. Lugovitskaya, D. A. Rogozhnikov and S. V. Mamyachenkov, *J. Mol. Liq*., **417**, 126693 (2024), https://doi.org/10.1016/j.molliq.2024.126693
[13] G. Milczarek, T. Rebiś and J. Fabiańska, *Colloids Surf. B Biointerfaces*, **105**, 335 (2013), https://doi.org/10.1016/j.colsurfb.2013.01.010
[14] A. Modrzejewska-Sikorska, E. Konował, A. Cichy, M. Nowicki, T. Jesionowski and G. Milczarek, *J. Mol. Liq*., **240**, 80 (2017), https://doi.org/10.1016/j.molliq.2017.05.065
[15] L. Yin, J. Yang, L. Liu, B. Lu, X. Lyu *et al*., *Nanoscale*, **17**, 2451 (2025), https://doi.org/10.1039/D4NR04161E
[16] E. Konował, A. Modrzejewska-Sikorska and G. Milczarek, *Mater. Lett*., **159**, 451 (2015), https://doi.org/10.1016/j.matlet.2015.07.052
[17] B. Pang, J. Yan, L. Yao, H. Liu, J. Guan *et al*., *RSC Adv*., **6**, 9753 (2016), https://doi.org/10.1039/C5RA21434C
[18] I. Ali, *RSC Adv*., **8**, 30125 (2018), https://doi.org/10.1039/C8RA06517A
[19] M. Khnifira, S. El Hamidi, A. Mahsoune, M. Sadiq, G. Serdaroğlu *et al*., *Inorg. Chem. Commun*., **129**, 108659 (2021), https://doi.org/10.1016/j.inoche.2021.108659
[20] M. Khnifira, S. El Hamidi, A. Machrouhi, A. Mahsoune, W. Boumya *et al.*, *Desalin. Water Treat*., **190**, 393 (2020), https://doi.org/10.5004/dwt.2020.25737
[21] G. M. Taha, E. S. Mansor and M. Sultan, *Int. J. Biol. Macromol.*, **193**, 1859 (2021), https://doi.org/10.1016/j.ijbiomac.2021.11.018
[22] A. Arvinte, M. Ignat, M. Pinteala and L. Ignat, *Curr. Anal. Chem*., **13**, 370 (2017), https://doi.org/10.2174/1573411012666161102143930
[23] I. C. Marinas, L. Ignat, M. E. Ignat, M. D. Gaboreanu, A. Coroaba *et al*., *Heliyon*, **10**, e26047 (2024), https://doi.org/10.1016/j.heliyon.2024.e26047
[24] S. Hu and Y.-L. Hsieh, *Carbohyd. Polym*., **131**, 134 (2015), https://doi.org/10.1016/j.carbpol.2015.05.060
[25] E. K. Vydhehi, V. C. Saheer, A. Thayyullathil, N. Subair and T. M. Anjana, *Fibers Polym*., **27**, 793 (2026), https://doi.org/10.1007/s12221-025-01248-w
[26] H. Chakhtouna, H. Benzeid, N. Zari, A. E. K Qaiss and R. Bouhfid, *Environ. Sci. Pollut. Res*., **28**, 44638 (2021), https://doi.org/10.1007/s11356-021-14996-y
[27] D. Kanakaraju, F. D. A. Kutiang, Y. C. Lim and P. S. Goh, *Appl. Mater. Today*, **27**, 101500 (2022), https://doi.org/10.1016/j.apmt.2022.101500
[28] H. Sadeghifar and A. Ragauskas, *Polymers*, **12**, 1134 (2020), https://doi.org/10.3390/polym12051134
[29] S. Y. Oh, D. I. Yoo, Y. Shin and G. Seo, *Carbohyd. Res*., **340**, 417 (2005), https://doi.org/10.1016/j.carres.2004.11.027
[30] A. Refaat, H. Elhaes and M. A. Ibrahim, *Sci. Rep*., **13**, 21649 (2023), https://doi.org/10.1038/s41598-023-48850-7
[31] Y. Qin, D. Yang, F. Gu, X. Li, W. Xiong *et al.*, *Sustain. Chem. Process*., **4**, 5 (2016), https://doi.org/10.1186/s40508-016-0050-0
[32] E. A. Karpukhina, D. S. Volkov and M. A. Proskurnin, *Agronomy*, **13**, 1141 (2023), https://doi.org/10.3390/agronomy13041141
[33] Y. D. Chai, Y. L. Pang, S. Lim, W. C. Chong, C. W. Lai *et al*., *Polymers*, **13**, 3530 (2021), https://doi.org/10.3390/polym13203530
[34] K. Maślana, A. Żywicka, K. Wenelska and E. Mijowska, *Int. J. Mol. Sci*., **22**, 1451 (2021), https://doi.org/10.3390/ijms22031451
[35] Y. Zhang, J. Hao, H. Zhao, W. Zhang, G. Shi *et al.*, *ACS Sustain. Chem. Eng*. **11**, 11130 (2023), https://doi.org/10.1021/acssuschemeng.3c01719
[36] K. Plermjai, K. Boonyarattanakalin, W. Mekprasart, W. Phoohinkong, S. Pavasupree *et al*., *Chiang Mai Journal of Science*, **46**, 618 (2019)
[37] Y. Chen, Z. Xiang, D. Wang, J. Kang and H. Qi, *RSC Adv*., **10**, 23936 (2020), https://doi.org/10.1039/d0ra04509h
[38] A. G. Thomas and K. L Syres, *Chem. Soc. Rev*., **41**, 4207 (2012), https://doi.org/10.1039/C2CS35057B
[39] A. D. French, *Cellulose*, **21**, 885 (2014), https://doi.org/10.1007/s10570-013-0030-4
[40] L. Segal, J. J. Creely, A. E. Martin and C. M. Conrad, *Text. Res. J.*, **29**, 786 (1959), https://doi.org/10.1177/004051755902901003
[41] R. Verma, J. Gangwar and A. K. Srivastava, *RSC Adv*., **7**, 44199 (2017), https://doi.org/10.1039/c7ra06925a
[42] J. Chen, M. Guan, X. Zhang and X. Gong, *RSC Adv*., **9**, 36615 (2019), https://doi.org/10.1039/c9ra07483j
[43] R. Majumdar and P. K. Kar, *Sci. Rep*., **13**, 7415 (2023), https://doi.org/10.1038/s41598-023-34221-9

[44] L. Sherpa, A. Nimmala and S. V. S. N. Rao, *Discover Nano*, **19**, 51 (2024), https://doi.org/10.1186/s11671-024-03994-x
[45] D. G. Gray and X. Mu, *Materials*, **8**, 7873 (2015), https://doi.org/10.3390/ma8115427
[46] L. Villar, M. Pita, J. Paez and P. B. Sánchez, *Cellulose*, **30**, 3027 (2023), https://doi.org/10.1007/s10570-022-05036-0
[47] L. G. Thygesen, B. J. Hidayat, K. S. Johansen and C. Felby, *J. Ind. Microbiol. Biotechnol.*, **38**, 975 (2011), https://doi.org/10.1007/s10295-010-0870-y
[48] S. Bakhta, Z. Sadaoui, N. Boudechiche, H. Hafsa, K. Sellami *et al.*, *RSC Adv.*, **15**, 38435 (2025), https://doi.org/10.1039/D5RA05466D
[49] L. Nouri, S. Hemidouche, A. Boudjemaa, F. Kaouah, Z. Sadaoui *et al.*, *Int. J. Biol. Macromol.*, **151**, 66 (2020), https://doi.org/10.1016/j.ijbiomac.2020.02.159